Available online at www.sciencedirect.com
SCIENCE DIRECT®
Ultrasonics 43 (2005) 457–465
Ultrasonics
www.elsevier.com/locate/ultras

Three-dimensional modelling of micromachined-ultrasonic-transducer arrays operating in water

Mikaël Wilm *, Alexandre Reinhardt, Vincent Laude, Raphaël Armati, William Daniau, Sylvain Ballandras

Département LPMO, Institut FEMTO-ST, CNRS UMR 6174, 32 avenue de l'Observatoire, 25044 Besançon Cedex, France

Received 6 September 2004; accepted 18 September 2004
Available online 19 October 2004

Abstract

We report on the 3-D modelling of periodic arrays of capacitive micromachined ultrasonic transducers (cMUTs) operating in fluid. Specific developments have been performed to model biperiodic transducer arrays and to take into account radiation into any stratified media at the front-side as well as the back-side of the device. The model is based on a periodic finite-element-analysis/boundary-element-method (FEA/BEM). It is applied to micromachined ultrasonic transducers (MUTs), based on silicon-nitride-circular-membrane arrays on a silicon substrate, and operating in water. The spectrum characteristics of MUTs excited in phase are investigated, showing that very-large-band emission is achievable as previously demonstrated by many authors. However, other contributions are also found, depending on the excitation conditions, that do not radiate in the fluid. These contributions are identified as guided modes that could generate significant cross-talk effects. The origin and the nature of these modes is analyzed to gain insight in the actual operation of MUTs.
© 2004 Elsevier B.V. All rights reserved.

PACS: 43.38.Hz; 43.38.Dv; 43.40.Rj; 43.40.Dx
Keywords: Micromachined ultrasonic transducer; Array; Radiation; Cross-talk

1. Introduction

Until now, modern ultrasonic transducer arrays for medical imaging systems are mainly based on piezoelectric composite structures, consisting in an association of materials of various natures (ceramics, polymers, metals) [1]. Recently, micromachined ultrasonic transducers (MUTs) have appeared as an alternative to such structures and give rise to new opportunities in the development of high-density integrated imaging devices. The capability of such devices to make images has been proved [2,3] with a better axial resolution but a sensitivity that still has to be improved. Sensors and actuators based on MUTs also have demonstrated their potential for microfluidic applications [4].

Nevertheless, strong limitations may arise for phased-array applications, due to strong cross-coupling in MUT structures, caused by Lamb waves or surface waves propagating in the substrate, interface waves between the transducer and the radiation medium. Solutions have been proposed [5] to reduce some of the cross-talk phenomena, as undercuts or applying a collapse voltage to non-active cells.

However, the behavior complexity of MUTs requires that their modelling takes into account the massively-periodic nature of the arrays, the radiation media, as well as an accurate description of the device geometry, including membranes and cavities. To address that

* Corresponding author. Tel.: +33 3 81 85 39 78; fax: +33 3 81 85 39 98.
E-mail address: mikael.wilm@lpmo.edu (M. Wilm).

0041-624X/$ - see front matter © 2004 Elsevier B.V. All rights reserved.
doi:10.1016/j.ultras.2004.09.006

problem, we have implemented our own computation tool [6], based on finite-element analysis (FEA), by adding specific periodicity boundary conditions, and by coupling it to a boundary-element method (BEM) to include radiation media.

In Section 2, we recall the main lines of the periodic FEA/BEM. In Section 3, simulation results are presented, considering the pure mechanical behavior of MUT arrays, and are discussed. The well-known very-large-band emission of MUTs excited in phase is pointed out. Guided contributions are found, that propagate along the array, as in the case of a silicon/water system, such as Leaky-Rayleigh or leaky-Lamb waves (depending on the nature of the substrate), or Stoneley–Scholte waves. Membrane modes also propagate at the interface due to coupling between membranes by water. All these modes are theoretically found to contribute to cross-talk effects in the operating-frequency range, caused by resonant coupling between MUT cells. We conclude by discussing the way our simulations can be used to improve the typical characteristics of MUTs and particularly to minimize cross-talk effects.

2. Finite-element modelling

Based on the finite-element-analysis (FEA) toolbox from INRIA named Modulef [7], we have developed our own computation package [6] to simulate three-dimensional biperiodic piezoelectric devices and to take into account radiation conditions in any stratified media, mixing fluids and solids [8].

The scheme adopted for the present work relies on a mechanical displacement and electrical potential formulation (see for instance [9]) and addresses purely elastic or piezoelectric problems, so that piezoelectric MUTs also can be treated. Only the final form of the problem is recalled here.

Considering a monochromatic variation of mechanical and electrical fields with a time dependence $\exp(j\omega t)$ where ω is the angular frequency, the standard discrete form of the FEA is written in the case of the general piezoelectric problem [6]

$$\begin{bmatrix} K_{uu} - \omega^2 M_{uu} & K_{u\phi} \\ K_{\phi u} & K_{\phi\phi} \end{bmatrix} \begin{pmatrix} u \\ \phi \end{pmatrix} = \begin{pmatrix} F \\ Q \end{pmatrix}, \tag{1}$$

where K_{uu} and M_{uu} correspond to the stiffness and mass matrices of the purely elastic part of the problem, respectively, $K_{u\phi}$ is the piezoelectric-coupling matrix and $K_{\phi\phi}$ represents the purely dielectric part. u and ϕ are respectively the nodal displacements and electrical potential, and, in the right-hand side, F and Q are respectively relative to nodal mechanical and electrical loads.

2.1. Periodicity

Let us consider now a quasi-biperiodic transducer array, which elementary-cell geometry conforms to Fig. 1. The x_3-axis is assumed normal to the front of the device without any loss of generality.

We apply a harmonic excitation distribution, that is a mechanical force or an electrical potential, in the space domain [10], which is written as

$$\phi_{m,p} = \phi_0 \exp(-j2\pi(m\gamma_1 + p\gamma_2)), \tag{2}$$

where the phase varies linearly with m and p. This means that the (m,p)th cell of the array is excited by a potential or a force of magnitude ϕ_0 modulated by a phase proportional to its distance from the $(0,0)$th cell. γ_1 and γ_2 are called excitation parameters and vary in the range $[0;0.5]$ allowing for the coverage of the first Brillouin zone [11] of the system. They are respectively associated with periods d_1 and d_2 of the structure (see Fig. 1).

According to the Bloch–Floquet theory [11], all fields obey a quasi-periodicity law, yielding for instance the following mechanical displacements:

$$u_i(x_1 + md_1, x_2 + pd_2) = u_i(x_1, x_2)\mathrm{e}^{-j2\pi(m\gamma_1 + p\gamma_2)}. \tag{3}$$

This relation imposes the definition of specific boundary conditions at the limits of the unit cell shown in Fig. 1. These so-called periodicity conditions directly involve all degrees of freedom at the corresponding boundaries and are written [12,6]

$$\begin{aligned} u_{\Gamma_B} &= u_{\Gamma_A}\mathrm{e}^{-j2\pi\gamma_1}, \\ u_{\Gamma_D} &= u_{\Gamma_C}\mathrm{e}^{-j2\pi\gamma_2}, \\ u_{E_2} &= u_{E_1}\mathrm{e}^{-j2\pi\gamma_1}, \\ u_{E_3} &= u_{E_1}\mathrm{e}^{-j2\pi\gamma_2}, \\ u_{E_4} &= u_{E_1}\mathrm{e}^{-j2\pi(\gamma_1+\gamma_2)}, \end{aligned} \tag{4}$$

where E_i are relative to the corners of the unit cell and Γ_A to Γ_D are relative to the sides excluding the corners. One has to note that the spatial distribution of nodes along the boundaries must be identical for each couple of sides to ensure the consistancy of Eqs. (4). A variable change is then performed by writing (for more details, see Ref. [6])

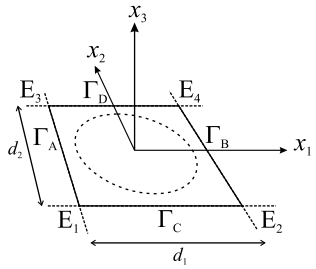

Fig. 1. Simplified geometry of the unit cell of a biperiodic MUT array.

$$
\begin{aligned}
v_{\Gamma_A} &= u_{\Gamma_A},\\
v_{\Gamma_B} &= u_{\Gamma_B} - u_{\Gamma_A}\mathrm{e}^{-j2\pi\gamma_1},\\
v_{\Gamma_C} &= u_{\Gamma_C},\\
v_{\Gamma_D} &= u_{\Gamma_D} - u_{\Gamma_C}\mathrm{e}^{-j2\pi\gamma_2},\\
v_{E_1} &= u_{E_1},\\
v_{E_2} &= u_{E_2} - u_{E_1}\mathrm{e}^{-j2\pi\gamma_1},\\
v_{E_3} &= u_{E_3} - u_{E_1}\mathrm{e}^{-j2\pi\gamma_2},\\
v_{E_4} &= u_{E_4} - u_{E_1}\mathrm{e}^{-j2\pi(\gamma_1+\gamma_2)}.
\end{aligned}
\tag{5}
$$

The standard discrete form of Eq. (1) becomes

$$
\begin{bmatrix} \overline{C_u} & 0 \\ 0 & \overline{C_\phi} \end{bmatrix}^{\mathrm{T}} \begin{bmatrix} K_{uu} - \omega^2 M_{uu} & K_{u\phi} \\ K_{\phi u} & K_{\phi\phi} \end{bmatrix} \times \begin{bmatrix} C_u & 0 \\ 0 & C_\phi \end{bmatrix} \begin{pmatrix} v \\ \varphi \end{pmatrix} = \begin{bmatrix} \overline{C_u} & 0 \\ 0 & \overline{C_\phi} \end{bmatrix}^{\mathrm{T}} \begin{pmatrix} F \\ Q \end{pmatrix}, \tag{6}
$$

where C_u and C_ϕ are the mechanical and electrical variable-change matrices. The periodicity boundary conditions and the variable-change result in additional Dirichlet conditions ($v_{\Gamma_B} = v_{\Gamma_D} = v_{E_2} = v_{E_3} = v_{E_4} = 0$). Superscript T and overlining respectively stand for matrix transposition and complex conjugation.

Thus, Eq. (6) must be solved for each triplet $(\omega, \gamma_1, \gamma_2)$, yielding for instance the calculation of the harmonic admittance $Y(\omega, \gamma_1, \gamma_2)$ (in the piezoelectric case) or the harmonic deflection $u_n(\omega, \gamma_1, \gamma_2)$ of the membrane. Finally, mutual admittances or deflections [10,6] can be computed according to

$$
H_{m,p}(\omega) = \int_0^1 \int_0^1 H(\omega, \gamma_1, \gamma_2)\mathrm{e}^{j2\pi m\gamma_1}\mathrm{e}^{j2\pi p\gamma_2}\,\mathrm{d}\gamma_1\,\mathrm{d}\gamma_2, \tag{7}
$$

where H stands for Y or u_n, or any harmonic field that we are able to compute (electrical charge Q, mechanical force F, and so on).

Due to the variable change, the linear system to be solved loses its symmetry. For non-lossy materials, it becomes hermitian, while for materials exhibiting acoustic or dielectric losses, it becomes complex general. Moreover, the periodicity boundary conditions notably enlarge the width of the band of the linear equation system, resulting in larger computation time. Nevertheless, this approach is much more favorable than the computation of very large FEA problems in terms of efficiency and accuracy. Furthermore, an adapted algorithm devoted to sparse LU factorization and developed by Davis and Duff [13] has been used for computing sparse matrix linear systems.

2.2. Radiation in fluids and solids

As previously, we consider a two-dimensional transducer array. The surface radiating in water is assumed to be flat. Only an elementary cell is meshed and the periodicity conditions described above are applied.

Let us now consider the initial variational equation limited to the purely elastic problem

$$
\begin{aligned}
&\int\int\int_\Omega \left(-\rho\omega^2 u_i\overline{\delta u_i} + \frac{\partial\overline{\delta u_i}}{\partial x_j}c_{ijkl}\frac{\partial u_l}{\partial x_k}\right)\mathrm{d}V\\
&\quad = \int\int_\Gamma \overline{\delta u_i}T_{ij}n_j\,\mathrm{d}S,
\end{aligned}
\tag{8}
$$

in which δu_i is the variational unknown and n_j is the outward normal to the boundary surface Γ on which the radiation boundary condition is applied.

The periodic approach allows one to introduce the concept of periodic Green's function [14,15], and the right-hand side of Eq. (8) can be rewritten by assuming pressure equilibrium at the fluid/structure interface,

$$
T_{ij}n_j = -Pn_i, \tag{9}
$$

with

$$
\begin{aligned}
P(x_1, x_2) = -\frac{1}{d_1 d_2}\int\int_\Gamma G^{\mathrm{p}}(x_1 - x_1', x_2 - x_2')\\
\times u_{\mathrm{norm}}(x_1', x_2')\,\mathrm{d}x_2'\,\mathrm{d}x_1',
\end{aligned}
\tag{10}
$$

where u_{norm} is the displacement normal to the radiation surface and G^{p} is the periodic Green's function of the fluid written

$$
\begin{aligned}
G^{\mathrm{p}}(x_1, x_2) = \sum_{m,p=-\infty}^{+\infty} \widetilde{G}(\gamma_1 + m, \gamma_2 + p, \omega)\\
\times \mathrm{e}^{-j\frac{2\pi}{d_1}(\gamma_1+m)x_1}\mathrm{e}^{-j\frac{2\pi}{d_2}(\gamma_2+p)x_2}.
\end{aligned}
\tag{11}
$$

The periodic Green's function is a Bloch–Floquet formulation of the classical Green's function, requiring the expression of the Green's function in the Fourier domain $\widetilde{G}$. Performing the FEA interpolation procedure, the right-hand side of Eq. (8) becomes

$$
\begin{aligned}
&\int\int_\Gamma \overline{\delta u_i}T_{ij}n_j\,\mathrm{d}S\\
&\quad = \frac{1}{d_1 d_2}\sum_{k,l=-\infty}^{+\infty}\Bigg[\widetilde{G}(\gamma_1 + k, \gamma_2 + l, \omega).\\
&\qquad \times \left(\sum_{e=1}^{E}\sum_{m=1}^{Nd(e)}\overline{\delta u_{\mathrm{norm}}^{(m,e)}}\int\int_{\Gamma_e} N_m(x_1, x_2)\mathrm{e}^{-j\frac{2\pi}{d_1}(\gamma_1+k)x_1}\right.\\
&\qquad \left.\times\, \mathrm{e}^{-j\frac{2\pi}{d_2}(\gamma_2+l)x_2}\,\mathrm{d}x_1\,\mathrm{d}x_2\right)\\
&\qquad \times \left(\sum_{\varepsilon=1}^{E}\sum_{n=1}^{Nd(\varepsilon)} u_{\mathrm{norm}}^{(n,\varepsilon)}\int\int_{\Gamma_\varepsilon} N_n(x_1', x_2')\mathrm{e}^{j\frac{2\pi}{d_1}(\gamma_1+k)x_1'}\right.\\
&\qquad \left.\times\, \mathrm{e}^{j\frac{2\pi}{d_2}(\gamma_2+l)x_2'}\,\mathrm{d}x_1'\,\mathrm{d}x_2'\right)\Bigg],
\end{aligned}
\tag{12}
$$

where N_m are the interpolation polynomials of finite element e exhibiting Nd nodes. E is the total number of finite elements.

The same approach is also applicable if the medium in which the structure radiates is a solid. As the fluid, which was not meshed, the homogeneous part of the substrate can be considered a radiation medium and we do not have to mesh it. Considering the general solid case, the periodic Green's function used above is replaced by a periodic Green's tensor so that the normal stresses are written

$$T_{ij}n_j = \frac{1}{d_1 d_2}\int\int_{\Gamma} G^{\mathrm{p}}_{ijk}(x_1 - x'_1, x_2 - x'_2) \times u_k(x'_1, x'_2)\,\mathrm{d}x'_1\,\mathrm{d}x'_2 n_j, \tag{13}$$

with

$$G^{\mathrm{p}}_{ijk}(x_1, x_2) = \sum_{m,p=-\infty}^{+\infty} \widetilde{G}_{ijk}(\gamma_1 + m, \gamma_2 + p, \omega) \times \mathrm{e}^{-j\frac{2\pi}{d_1}(\gamma_1+m)x_1}\mathrm{e}^{-j\frac{2\pi}{d_2}(\gamma_2+p)x_2}, \tag{14}$$

and the right-hand side of Eq. (8) becomes:

$$\begin{aligned}\int\int_{\Gamma} \overline{\delta u_i} T_{ij} n_j \,\mathrm{d}S &= \frac{1}{d_1 d_2}\sum_{m,p=-\infty}^{+\infty}\left[\widetilde{G}_{ijk}(\gamma_1 + m, \gamma_2 + p, \omega) n_j \right.\\ &\times \int\int_{\Gamma} \overline{\delta u_i}\mathrm{e}^{-j\frac{2\pi}{d_1}(\gamma_1+m)x_1}\mathrm{e}^{-j\frac{2\pi}{d_2}(\gamma_2+p)x_2}\,\mathrm{d}x_1\,\mathrm{d}x_2\\ &\left.\times \int\int_{\Gamma} u_k \mathrm{e}^{j\frac{2\pi}{d_1}(\gamma_1+m)x'_1}\mathrm{e}^{j\frac{2\pi}{d_2}(\gamma_2+p)x'_2}\,\mathrm{d}x'_1\,\mathrm{d}x'_2\right],\end{aligned} \tag{15}$$

before performing the FEA interpolation scheme.

In all considered cases, the Green's function in the Fourier domain is computed using the approach described in Ref. [8], which is based on a scattering-matrix method and dedicated to the analysis of piezoelectric, fluid, and metallic multilayers. Practically, the media in which the structure radiates can be either semi-infinite, finite (plates), or stratified, and can consist of any fluid or solid material combination.

The contribution of the radiating boundary to the global algebraic system of Eq. (6) consists in a frequency and excitation-parameter dependent matrix $X(\omega, \gamma_1, \gamma_2)$ related both to degrees of freedom and variational unknowns and consequently computed in the left-hand side, yielding

$$\begin{aligned}&\begin{bmatrix}\overline{C_u} & 0\\ 0 & \overline{C_\phi}\end{bmatrix}^{\mathrm{T}}\left[\begin{bmatrix}K_{uu} - \omega^2 M_{uu} & K_{u\phi}\\ K_{\phi u} & K_{\phi\phi}\end{bmatrix}\right.\\ &\left.-\begin{bmatrix}X_{uu} & X_{u\phi}\\ X_{\phi u} & X_{\phi\phi}\end{bmatrix}(\omega, \gamma_1, \gamma_2)\right] \times \begin{bmatrix}C_u & 0\\ 0 & C_\phi\end{bmatrix}\begin{pmatrix}v\\ \varphi\end{pmatrix}\\ &= \begin{bmatrix}\overline{C_u} & 0\\ 0 & \overline{C_\phi}\end{bmatrix}^{\mathrm{T}}\begin{pmatrix}F\\ Q\end{pmatrix}.\end{aligned} \tag{16}$$

This final algebraic system takes into account periodicities as well as radiation in a large variety of stratified media. The concept of harmonic and mutual quantities, such as harmonic and mutual admittances for the piezoelectric case or harmonic and mutual displacements, allows one to identify modes propagating in the structure, and to evaluate cross-talk effects and to identify their causes. This approach is applied to MUTs.

3. Results and discussion

In this section, we study a capacitive-like MUT by applying an harmonic force on its membrane, as would be caused by a capacitive excitation. In this calculation, we do not take into account the variation of the electrostatic force within the gap. Consequently, this work is dedicated to the analysis of the pure mechanical behavior of such a transducer array.

The studied cMUT consists in a silicon-nitride membrane, supposedly fabricated by surface micromachining, on a silicon substrate. The diameter of the membrane is 80 μm. The period of the cell is 90 μm. These dimensions have been chosen arbitrarily. Fig. 2 shows the typical unit-cell mesh for the silicon-nitride layer with the membrane. The back-side is in contact with the silicon substrate. Note that a two-degree-interpolation scheme is used in the FEA.

We first consider a synchronous excitation of the whole transducers of the array by fixing the excitation parameters γ_1 and γ_2 to zero. It means that the membranes are excited in phase with a force of constant magnitude. The substrate is considered semi-infinite, and the membrane is 1-μm thick. The air gap is 0.5 μm. Both cases of membranes radiating in a vacuum and in water

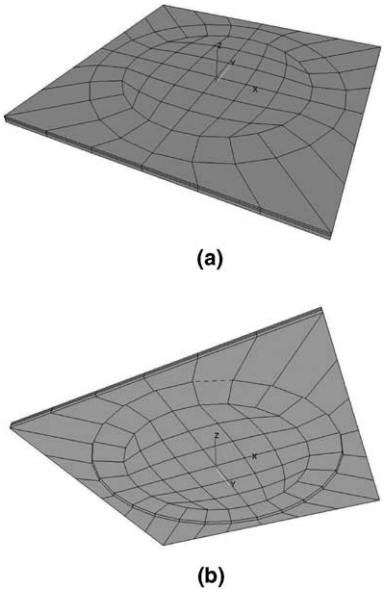

Fig. 2. Mesh of the unit-cell: front-side (a) and back-side (b) of the silicon-nitride layer with the membrane.

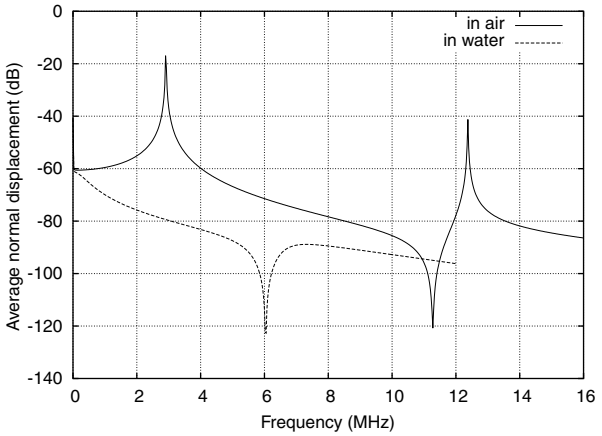

Fig. 3. Magnitude of the average normal deflection of the array of MUTs vibrating synchronously respectively in air and water.

are dealt with. Fig. 3 shows the harmonic average deflection of the membrane for both cases.

When vibrating in air, two very sharp resonances occur at 2.91 MHz and 12.37 MHz, corresponding to the fundamental flexural mode of the membrane and its harmonic, respectively denoted (0, 1) and (0, 2) in Fig. 4. By damping the membranes with water, the resonance frequencies are dramatically shifted down to low frequencies. Moreover the membrane array does not exhibit any more true-resonance contributions, inducing an intrinsic wide-bandwidth behavior. As has been shown for the one-dimensional-membrane case [16], the resonance frequencies of a unique membrane radiating in water are also shifted down, but the membrane still exhibits true resonances. The frequency shift increases together with the number of cells in the array, and the displacement magnitude decreases. At the same time, the resonance peaks are less and less marked, until their complete vanishing. One has to keep in mind that the considered quantity is the average displacement, which can be zero even if the membranes still vibrate. Considering the water-radiation case, the membranes vibrate according to the fundamental (0, 1) mode near 0 MHz, and the vibration slowly moves to the (0, 2) mode shape near 7 MHz, so that the average deflection is nearly zero for 6 MHz due to the particular shape of the (0, 2) mode.

Since the response of a membrane is highly dependent on its geometrical characteristics, the average velocity has been computed for different thicknesses from 0.5 μm to 1.5 μm, as reported in Fig. 5. In each case, the array still exhibits a wide-bandwidth behavior, and the membrane thickness will determine the working frequency.

Let us now assume a particular distribution of excitation forces. Considering Eq. (2), the excitation parameter γ_2 is fixed to zero and γ_1 is allowed to vary, which corresponds to rows of membranes excited with a phase $2\pi\gamma_1$ between neighboring rows. Fig. 6 represents the magnitude of the average harmonic deflection as a function of frequency and excitation parameter γ_1. Different kinds of contributions arise and have to be detailed. They are summarized in Fig. 7.

Two quasi-non-dispersive waves propagate along the x_1-axis, with velocities respectively around 1500 m s^{-1} and 4850 m s^{-1}. If one compares the structure to a silicon/water system, the first one is an interface wave [17] also called Stoneley–Scholte wave. This wave is evanescent in both media and is mostly localized in the water. The vibration shape of the membrane, associated to the Stoneley–Scholte wave, is that of the (1, 1) mode (see Fig. 4). Since the computations are performed for values of γ_1 reduced to the first Brillouin zone (γ_1 between 0 and 0.5), the interface wave seems to have an apparently-negative group velocity above 8.4 MHz. In that case, the membrane vibration shape is that of the (1, 2) mode of a circular membrane. The second contribution is a Rayleigh wave propagating in the substrate for a specific range of γ_1 in the operating-frequency range. Practically, it is induced by stresses applied to the substrate where the membranes are anchored, and its existence is related to the fact that acoustic waves in the silicon substrate are not directly damped by water but protected from it by the membranes. In that case, the pre-existent membrane vibration shape is not affected. Nevertheless, the Rayleigh wave is partially damped by the fluid wherever the substrate is not protected by the membranes. This induces leakage in the fluid and can affect the radiation pattern. On the opposite, the Stoneley–Scholte wave, mainly localized in the fluid, propagates along the structure without loss and is not responsible for leakage. However, the associated membrane vibration is capable of modifying the radiation pattern.

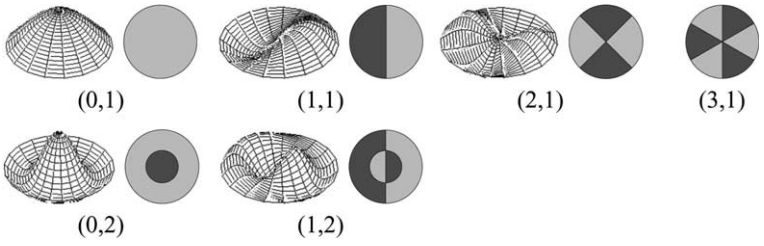

Fig. 4. Vibrational modes of circular drums. The nomenclature for labelling modes is (d, c) with d the number of nodal diameters and c the number of nodal circles where there is no displacement. Out-of-phase vibration lobes are represented for each mode.

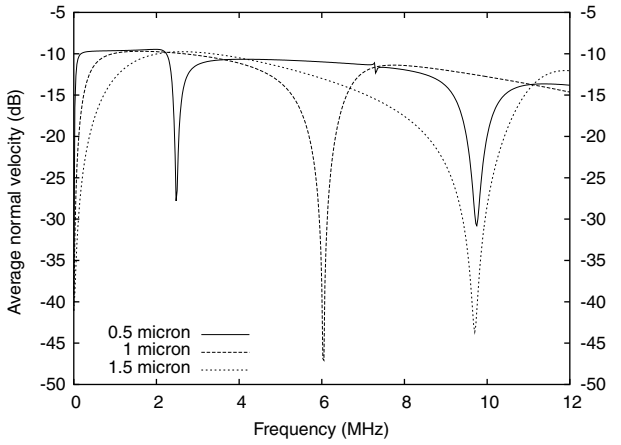

Fig. 5. Average normal velocity of the transducers computed for three different thicknesses of the membranes.

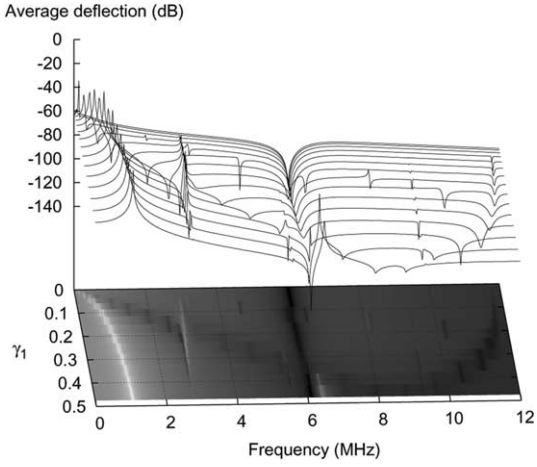

Fig. 6. Harmonic average normal deflection for the excitation parameter γ_1 varying from 0 to 0.5 ($\gamma_2 = 0$).

The other contributions, that are dispersive, are not due to the silicon/water-like system, but to the geometrical nature of the transducers, since their vibration shapes are related to the modes of a circular membrane. These latter modes are represented in Fig. 4 [18], and the modes associated to a specific contribution are indicated in Fig. 7. One has to note that modes, which do not exhibit a revolution symmetry, i.e. that are different from $(0, c)$, are almost not coupled by the excitation near γ_1 respectively equal to 0 and 0.5. Since they are almost not coupled when the array is operating in a vacuum whatever the value of γ_1, these resonant modes exist due to the presence of the fluid which acts as a coupling medium between neighboring membranes.

By separately plotting the real and imaginary parts of the average normal displacement, as depicted in Fig. 8, one has access to the radiating contributions. It is similar to the surface-acoustic-wave problem where the imaginary part of the charge indicates losses in the substrate, i.e. bulk waves radiating towards the substrate. One can see that no radiation occurs below a certain

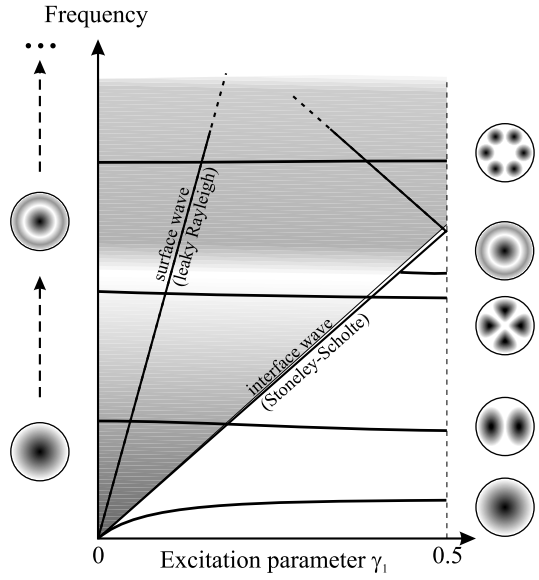

Fig. 7. Diagram exhibiting the dispersion curves of the resonant modes and the radiation area, considering a 1D-array of MUTs with circular membranes.

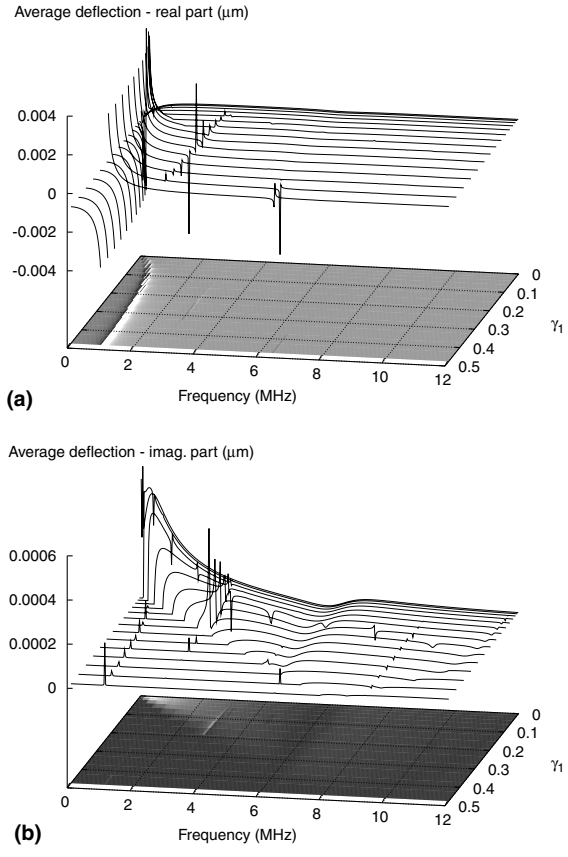

Fig. 8. Harmonic average deflection, (a) real part and (b) imaginary part, for γ_1 varying from 0 to 0.5 (with $\gamma_2 = 0$).

limit, that naturally corresponds to the group velocity in water. This limit reduces the bandwidth of the array when the excitation parameter γ_1 is different from zero, for instance in the case of beam steering. Since it only depends on the velocity of the fluid, the limit will be shifted down by an increase in the number of rows in one pixel, since all rows belonging to the same pixel will be excited in phase, i.e. by an increase in the period of the array. Nevertheless, one has to take care that the number of MUT rows per pixel does not exceed a certain value to avoid secondary lobes in the radiation pattern [19]. Furthermore, the fundamental mode and its harmonic are resonant again below this limit, whereas the other membrane modes are resonant even in the radiation area even if they are partially damped by the fluid.

Until now, the silicon substrate was considered semi-infinite and a Rayleigh wave has been shown to propagate along the array. In practice, one does not work with semi-infinite substrates, but with 380–500-μm thick silicon plates. Since these wafers could be capable to guide plate modes for wavelengths similar to those of the surface wave, the finite-thickness-substrate case has been computed in order to see what actually happens. In the following calculation, a 480-μm-thick plate is considered instead of the semi-infinite substrate. Note again that we do not need to mesh the plate thanks to the boundary-element part of the method, the plate being taken into account by the scattering-matrix part [8].

Comparing with the semi-infinite-substrate case, the Rayleigh-like wave does not exist any more, but additional waves appear on the average harmonic normal velocity reported in Fig. 9a. Fig. 9b shows the dispersion curves of a 480-μm-thick plate of silicon. One can identify the symmetric modes S_0 and S_1, and the anti-symmetric A_0 and A_1 modes [20]. The superimposition of the computed harmonic-displacement diagram and the classical Lamb-waves dispersion curves shows that the observed contributions are effectively due to Lamb waves propagating in the structure. As in the Rayleigh-wave case, these waves are generated by membrane displacements that induce stresses at their edges, where they are anchored to the substrate. The presence of the fluid domain will induce leakage of the Lamb waves, so that the radiation pattern will be affected, as has been shown experimentally by Jin et al. [5]. With the considered thickness, only the S_0 and A_0 modes can modify the radiation pattern since the other Lamb modes are localized outside the bandwidth of the array.

For both cases of semi-infinite or finite-thickness substrate, the parasitic modes precedently described are expected to degrade the operation of MUT arrays, since they are able to induce cross-coupling effects, and to affect the radiation pattern. This is numerically investigated next thanks to the concept of mutual quantities [10,6] described in Section 2.1.

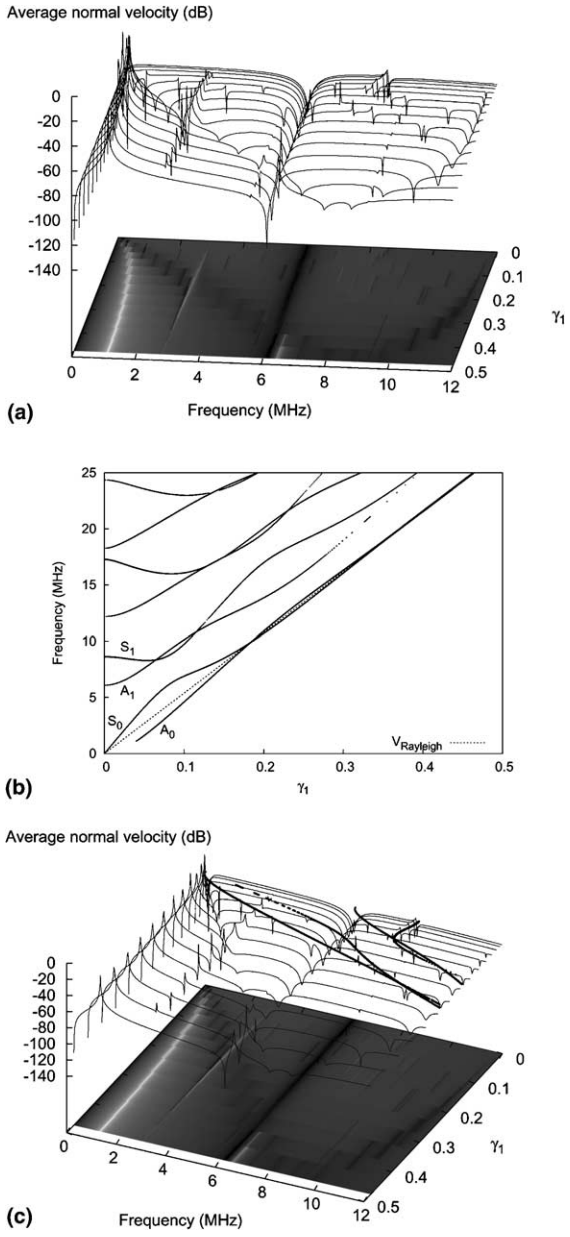

Fig. 9. (a) Average harmonic normal velocity in the case of a finite-thickness substrate, (b) dispersion curves of the equivalent silicon plate, (c) superimposition of the two curves.

By a numerical integration, we compute the mutual displacements or velocities in the semi-infinite-substrate case. Computations are performed by taking thirty integration points and using a Gauss rule. The integration result is shown in Fig. 10.

In the operation-frequency range, for non-resonant-operation regimes, the radiating average-normal-velocity contribution exhibits a 10 dB decrease between the excited row and its neighbor, and then between the two first neighboring rows. Since it is not a resonant contribution, it fades very quickly when propagating along the structure.

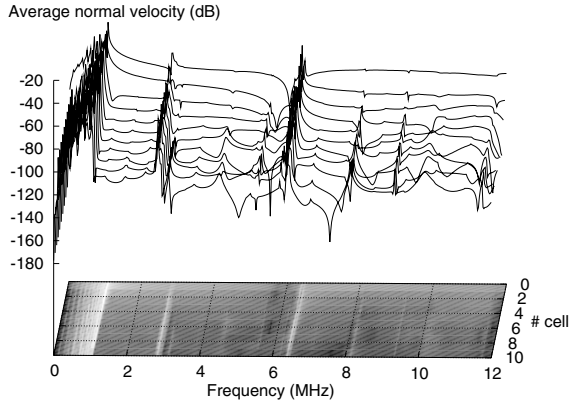

Fig. 10. Average mutual normal velocity between the excited cell row and its first 10 neighboring rows.

Strong cross-talks arise at low frequency until 1.05 MHz, which is the cut-off frequency of the resonant mode $(0,1)$, reported in Fig. 7. For a given frequency below this cut-off frequency, the mode propagates along the structure with a group velocity given by $\frac{\partial\omega}{\partial k_1} = d_1 \frac{\partial f}{\partial \gamma_1}$. Due to multiple partial reflections of the mode on the different neighboring rows, constructive or destructive interferences occur, resulting in periodic ripples under the cut-off frequency. At the cut-off frequency, the wave enters its Bragg condition, so that all the rows vibrate, two neighboring rows vibrating out-of-phase. In that case, the wavelength is twice the period of the array. Since this mode can be shifted to low frequencies by increasing the number of MUT rows per electric pixel, the induced cross-talks can be shifted down out of the operation-frequency range.

Near 8 MHz, the mutual admittances exhibit another contribution. That latter is due to the Stoneley–Scholte wave that enters its Bragg condition.

Other contributions due to the resonant modes described before arise at localized frequencies. By shifting down the radiation limit, mode $(0,2)$ is entirely localized in the radiation area, and does not have a resonant behavior any more whatever the value of γ_1. What is more dramatic is the leaky resonant mode $(1,1)$ localized in the middle of the bandwidth near 3 MHz, that exists whatever the radiation limit. As explained before, this mode is due to membrane coupling by the fluid. The propagation of this mode along the structure generates cross-talks that can strongly affect the radiation pattern and so the operation of MUT arrays.

4. Conclusion

We have reported on a flexible and robust method dedicated to the simulation of multi-periodic three-dimensional transducers radiating in an arbitrary stratified medium. It is based on a spectral finite-element analysis/boundary-element method. Concepts of harmonic and mutual quantities, such as displacements, have been introduced, and related specific boundary conditions have been added to describe the periodical nature of the structures. A boundary-element method associated with the concept of periodic Green's function has been added to the FEA to take into account radiation in a variety of media such as water or silicon substrates.

We have used this computation tool to simulate and analyze the operation of micromachined-ultrasonic-transducer 1D arrays operating in water. Contrarily to standard piezoelectric bulk transducers, MUTs do not operate on a resonant mode. These devices are massively periodic and hence subject to acoustic cross-talk phenomena when radiating in water. These features make them particularly suited to be analyzed using the proposed developments. An operation, analogous to that of a water/silicon system, is first observed in terms of surface acoustic waves (semi-infinite substrate) or plate waves, and of interface waves, that latter being mainly localized in the fluid. By taking into account the geometry of the structure, computations show a coupling of the membranes through water. Although they are damped by the fluid, the resulting modes exhibit resonances that induce cross-talk phenomena also in the operation-frequency range. That latter phenomenon can explain problems encountered when using MUT arrays as phased arrays. Our approach allows one first to understand what happens in the structure due to periodicity and fluid damping, then to identify crucial parameters for the design of ultrasound probes based on MUTs.

Acknowledgment

The authors would like to thank J.-F. Gelly, R. Lardat, W. Steichen, and F. Lantéri for fruitfull discussions, GE Parallel Design SAS and Framatome ANP for their financial support.

References

[1] W.A. Smith, The role of piezocomposites in ultrasonic transducers, in: Proc. of the IEEE Ultrasonics Symposium, 1989, pp. 755–766.
[2] Ö. Oralkan, A. Sanli Ergun, J.A. Johnson, M. Karaman, U. Demirci, K. Kaviani, Th.H. Lee, B.T. Khuri-Yakub, Capacitive micromachined ultrasonic transducers: next-generation arrays for acoustic imaging?, IEEE Trans. Ultrason., Ferroelect., Freq. Contr. 49 (11) (2002) 1596–1610.
[3] D.M. Mills, S. Smith, Real-time in-vivo imaging with capacitive micromachined ultrasound transducer (cMUT) linear arrays, in: Proc. of the IEEE Ultrasonics Symposium, 2003, pp. 568–571.
[4] J. McLean, F.L. Degertekin, Interdigital capacitive micromachined ultrasonic transducers for microfluidic applications, in: Proc. of the IEEE Ultrasonics Symposium, 2003, pp. 589–592.
[5] X. Jin, Ö. Oralkan, F. Levent Degertekin, B.T. Khuri-Yakub, Characterization of one-dimensional capacitive micromachined

ultrasonic immersion transducer arrays, IEEE Trans. Ultrason., Ferroelect., Freq. Contr. 48 (3) (2001) 750–760.
[6] S. Ballandras, M. Wilm, P.-F. Edoa, A. Soufyane, V. Laude, Finite-element analysis of periodic piezoelectric transducers, J. Appl. Phys. 93 (1) (2003) 702–711.
[7] Official Modulef web site, http://www-rocq.inria.fr/modulef/.
[8] A. Reinhardt, Th. Pastureaud, S. Ballandras, V. Laude, Scattering matrix method for modeling acoustic waves in piezoelectric, fluid, and metallic multilayers, J. Appl. Phys. 94 (10) (2003) 6923–6931.
[9] R. Lerch, Simulation of piezoelectric devices by two-and three-dimensional finite elements, IEEE Trans. Ultrason., Ferroelect., Freq. Contr. 37 (2) (1990) 233–247.
[10] Y. Zhang, J. Desbois, L. Boyer, Characteristic parameters of surface acoustic waves in a periodic metal grating on a piezoelectric substrate, IEEE Trans. Ultrason., Ferroelect., Freq. Contr. 40 (3) (1993) 183–192.
[11] L. Brillouin, Wave Propagation in Periodic Structures, Dover, New York, 1953.
[12] P. Langlet, A.C. Hladky-Hennion, J.N. Decarpigny, Analysis of the propagation of plane acoustic waves in passive periodic materials using the finite element method, J. Acoust. Soc. Am. 98 (5) (1995) 2792–2800.
[13] T.A. Davis, I.S. Duff, An unsymmetric-pattern multifrontal method for sparse LU factorization, SIAM J. Matrix Anal. Appl. 18 (1) (1997) 140–158.
[14] V.P. Plessky, Th. Thorvaldsson, Periodic green's functions analysis of SAW and leaky SAW propagation in a periodic system of electrodes on a piezoelectric crystal, IEEE Trans. Ultrason., Ferroelect., Freq. Contr. 42 (2) (1995) 280–293.
[15] P. Ventura, J.-M. Hodé, M. Solal, A new efficient combined FEM and periodic green's function formalism for the analysis of periodic saw structures, in: Proc. of the IEEE Ultrasonics Symposium, 1995, pp. 263–268.
[16] S. Ballandras, A. Caronti, W. Steichen, M. Wilm, V. Laude, Th. Pastureaud, R. Lardat, W. Daniau, Simulation of cMUT radiating in water using a mixed finite element/boundary element approach, in: Proc. of the IEEE Ultrasonics Symposium, 2002, pp. 1048–1051.
[17] I.A. Viktorov, Rayleigh and Lamb Waves, Plenum Press, 1967.
[18] Dr. Russell's homepage, http://www.kettering.edu/drussell/.
[19] L.J. Ziomek, Fundamentals of Acoustic Field Theory and Space-Time Signal Processing, CRC Press, 1995 (Chapter 7).
[20] D. Royer, E. Dieulesaint, Elastic Waves in Solids 1, Springer-Verlag, 2000.